**Proceedings of the ASME 2018**
**Dynamic Systems and Control Conference**
**DSCC2018**
**September 30-October 3, 2018, Atlanta, Georgia, USA**

**DSCC2018-8963**

# A BOWDEN CABLE-BASED SERIES ELASTIC ACTUATION MODULE FOR ASSESSING THE HUMAN WRIST

**Andrew Erwin**[*]**, Nick Moser, Craig. G. McDonald, and Marcia K. O'Malley**
Mechatronics and Haptic Interfaces Laboratory
Department of Mechanical Engineering
Rice University
Houston, Texas 77005
Email: ace7@rice.edu

## ABSTRACT

*Currently, wrist passive stiffness and active range of motion, two clinically relevant properties, are assessed using devices designed for rehabilitation. As a result, these devices do not have sufficient torque output and range of motion for complete wrist biomechanical assessment. To address these limitations, we are developing an actuation module specifically for assessing wrist biomechanical properties. Our device employs a serial kinematic exoskeletal architecture to directly interact with and measure wrist flexion/extension and radial/ulnar deviation. A Bowden cable-based actuation scheme, locating the motors off-board, was adopted for increased device range of motion and torque output compared with previous wrist exoskeletons. Additionally, the device was designed to incorporate a rotational elastic element at each joint, creating series elastic actuators, for accurate torque control and direct torque measurement. In this work, we present the design and demonstration of a 1-DOF module of the device, which can interact with a user's wrist in flexion/extension, providing an important first step towards the control, evaluation, and application of the 2-DOF device.*

## 1 INTRODUCTION

Robots have been deployed in the clinical setting for rehabilitation of individuals with neurological disorders, such as spinal cord injury or stroke [1]. Although robots have demonstrated their potential for rehabilitation in the clinic [2, 3], robot-aided assessments have yet to become as integrated [4]. Currently, only human-administered assessments, such as the prominent Fugl-Meyer Assessment, are accepted in clinical practice [5]. However, the Fugl-Meyer Assessment scale is labor-intensive, subjective, and graded on an ordinal scale. In contrast, robot-aided assessment offers the possibility for automated, objective, and high resolution assessments [4, 6]. Assessment robots might be used to improve our understanding of motor control and brain plasticity to improve robotic rehabilitation.

To further our understanding of motor recovery after neurological injury, studies have evaluated joint properties, such as passive stiffness. Passive stiffness of the wrist has previously been studied through robotic assessment with able-bodied participants [7, 8]. Stiffness of the wrist is especially important for rehabilitation, biomechanical modeling, and biologically inspired designs, since stiffness dominates wrist impedance [9]. Wrist rehabilitation is also appealing since studies have observed improvements in proximal joints during distal wrist training [10], although the training of proximal joints has not been observed to improve distal joints [2].

Prior wrist robotic devices have limitations in range of motion, torque output, and torque estimation accuracy, as a result of being originally designed for robot-aided rehabilitation, and not robot-aided assessment [11]. The only current study which used a wrist device for estimating wrist stiffness and range of motion was carried out using cadavers, additionally, the device is only suitable for cadavers [12]. In this work, we present details of a one-degree-of-freedom (DOF) module design for a 2-DOF wrist

[*]Address all correspondence to this author.

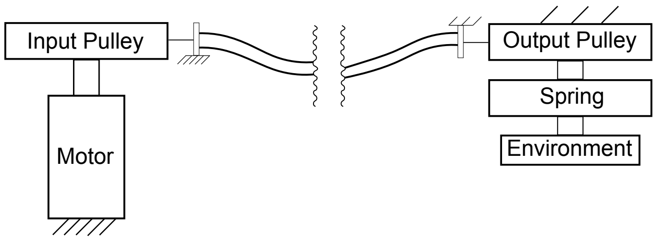


**FIGURE 1**. Block diagram of the implemented series elastic Bowden cable actuation scheme. By using series elastic actuation, direct torque measurement is achieved in addition to implementation of a transparent zero force control mode despite significant friction in the transmission. Note that in this work, two motors and pulleys are used on the input side. Compared with the case of using one motor per joint, using two motors eliminates the need for pre-tensioning mechanisms for the cables, and thereby also reduces static friction between the cable and conduit.

stiffness and range of motion assessment device. We chose to develop a device for such biomechanical wrist assessments due to the wrist's importance in performing many activities of daily living [13, 14]. The 1-DOF assessment module is demonstrated in a case study, which presents the intended protocol for wrist passive stiffness and active range of motion assessment.

## 2 Series Elastic Actuation for a 1-DOF Wrist Module

With reference to seminal wrist assessment studies [7, 8, 12] and rehabilitation devices [11, 15, 16], we identified the following requirements as paramount to develop a 2-DOF wrist stiffness and range of motion assessment device: 1) increase range of motion, 2) increase torque output, and 3) incorporate direct torque measurement. A Bowden cable-based actuation scheme, which locates the motors off-board as used in [17, 18], was adopted for increased device range of motion and torque output. However, the benefits of using Bowden cables comes at the cost of reduced accuracy in torque measurement and control. As a result, the module was designed to incorporate a rotational elastic element at each joint (see Fig. 1), creating series elastic actuators [19] for accurate torque control and direct torque measurement.

An essential component of the 1-DOF module is the series elastic element. The elastic element chosen for the module is a double Archimedes spiral rotational spring, similar to [20, 21]. This design is advantageous for this application since it is customizable and largest in the radial direction where space constraints are less problematic than in the longitudinal direction. To measure the deflection of the spring, US Digital's EM2 transmissive optical encoder module (EM2-2-10000-I) with a 50.8 mm diameter transmissive rotary hubdisk (HUBDISK-2-10000-375-IE) was selected. The encoder has 10,000 cnt/rev, which, with quadrature encoding, leads to a position resolution of $1.57 \cdot 10^{-4}$ rad. A nominal desired torque resolution of 10 N·mm was chosen, which results in a spring rate of 64 N·m/rad. Given the relative softness of the desired spring constant compared with other work which used steel springs, we elected to pursue a design using aluminum (7075-T651). Aluminum 7075-T651 has an excellent strength-to-weight ratio and a similar yield strength to steel, with approximately a third of the material stiffness.

To achieve the desired spring rate, an iterative design process using 3D computer-aided design (CAD) software was employed. This process considered the relationship between various parameters, such as the spring's spiral radius, width, thickness, and effective length. Note that the effective length is a function of the spiral's inner and outer fillet radii, as well as the number of spirals. These variables are illustrated in Fig. 2. The relationship between the variables and the spring constant is similar to that of a beam in bending with

$$k \propto \frac{Etw^3}{rl_e} \tag{1}$$

where $k$ is the spring constant, $E$ the material's Elastic Modulus, $t$ thickness, $w$ spiral width, $r$ spiral radius, and $l_e$ effective spiral length. By determining the spring constant for a single spring, this relationship can be used to rapidly modify the design for a different spring rate. Additionally, from a preliminary spring design, an offset of approximately 30% was determined between a finite element analysis estimate and the measured spring rate.

The iterative design process resulted in a spring with the physical parameters shown in Table 1. A finite element analysis of this spring estimated a spring rate of 73 N·m/rad, which was intentionally larger than the nominal desired 64 N·m/rad, since we prioritized not undershooting the spring rate. Additionally, the analysis led to a predicted maximum stress of 326 MPa at the maximum torque of 3 N·m (see Fig. 3). With the yield strength of aluminum 7075-T651 being approximately 505 Mpa, this provides a 1.5x safety factor, acceptable for the given application. An image of the manufactured spring, which was created through computer numerical machining, is shown in Fig. 2.

To evaluate the physical spring constant, a custom testbed was designed (see Fig. 4). The testbed consisted of a torque sensor, which was mechanically grounded on one side, while the other was rigidly connected to the outer race of the spring through a plate with the same bolt patterns of the load side pulley used in the final assembly. The inner race of the spring was connected to a shaft which was able to rotate freely through the use of a radial ball bearing. A handle was connected to the shaft

**TABLE 1**. Spring Specifications

| $r$ [mm] | $w$ [mm] | $t$ [mm] | $f$ [mm] | $s$ |
|---|---|---|---|---|
| 30.48 | 2.654 | 4.826 | 1.143 | 1 |

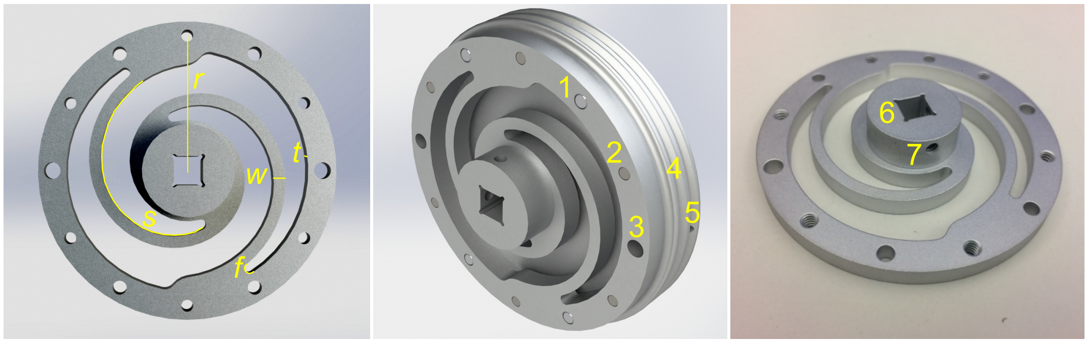


**FIGURE 2**. Custom-designed double Archimedes spiral spring. (left) CAD rendering including key physical dimensions: spiral radius ($r$), spiral width ($w$), spiral thickness ($t$), inner and outer fillet radius ($f$), and number of spirals ($s$). (center) CAD rendering including the connection to the output pulley. The two components are connected through 4x dowel pins (1) and 6x 6-32 screws (2). In addition, the spring includes a thru-hole for the set screw which secures the end of the cable (3). The cable runs in a race (4) in the pulley which includes an end cable hole (5). (right) Physical spring with an integrated hub (6) and 2x (one is not visible) 90° offset threaded set screws holes (7) for mating with the output shaft.

to enable an experimenter to provide the necessary 3 N·m torque. An encoder mounted on the same part which housed the ball bearing, measured the deflection of the spring since the other side of the spring was mechanically fixed.

The torque sensor used as a ground truth torque measurement during the static spring rate characterization was Transducer Techniques TRT-50-in-lb. The TRT-50-in-lb torque sensor can measure torque up to 5.649 N·m, with a safe overload of 150%, a rated output of 2 mV/V, nonlinearity and hysteresis of 0.1% of the rated output, and nonrepeatability of 0.05% of the rated output. The torque sensor's output voltage needs further

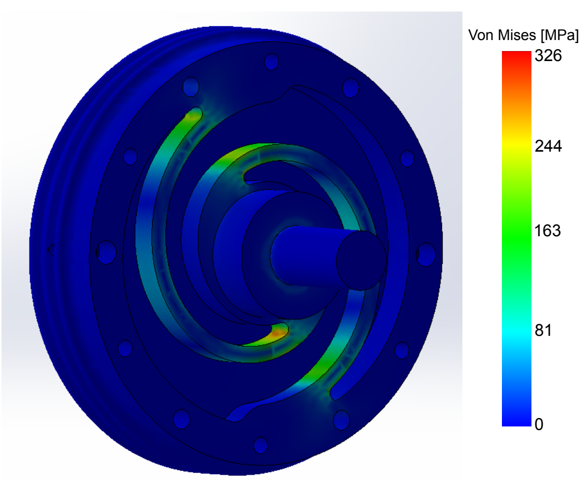


**FIGURE 3**. Finite element analysis static simulation of the spring in response to a 3 N·m torque applied to the pulley with the output shaft fixed. A color bar indicates the amount of Von Mises stress, maximum of 326 MPa, throughout the spring.

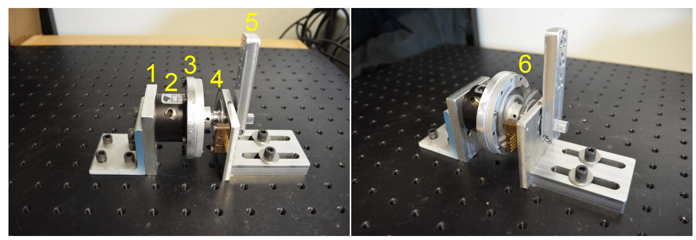


**FIGURE 4**. Testbed used to determine the spring constant. The testbed consists of 1) mechanical ground, 2) torque sensor, 3) spring plate, 4) encoder, 5) handle, and 6) spring. The encoder measures spring displacement while the torque sensor measures torque applied through the handle, which transmits torque through a radial ball bearing (not visible). The ground side is rigidly secured such that only spring displacement needs to be measured.

amplification before being sent to the data acquisition board, and so was amplified through an inverting amplification circuit using an AD620 operational amplifier. The gain of the amplification was set to 100.46.

To determine the spring constant, an experimenter applied torque to the spring through the handle in a quasi-static manner. The experimenter applied approximately 3 N·m of torque in each direction. The result of this experiment is presented in Fig. 5, which plots the torque vs. displacement of the spring. As can be seen, the spring deflection provides an accurate and linear estimate of torque. The resulting spring rate, $k$ = 75.96 N·m/rad, matches the adjusted finite element analysis estimate (73 N·m/rad) very closely. The experiment with the spring demonstrated a coefficient of determination ($R^2$) of 0.9998 with an average error of 0.012 N·m and a maximum full scale output error of 2.06%. As an indication of the quasi-static loading applied by the experimenter during the experiment, the mean rotational velocity was 0.0065 rad/s with a maximum velocity of 0.038 rad/s.

Note that unlike most other double spiral springs, the rotational spring in this work was made from aluminum (7075-T651) for a softer design, compared to steel, while still maintaining sufficient maximum torque. Additionally, the spring was created through computer numerical control machining, as opposed to the ubiquitous wire electrical discharge machining. Using computer numerical control machining enabled a design with the spring and spring hub, which mates with the output shaft, to be made as one piece, thus reducing mechanical play due to the small screws that would have been necessary to connect the two parts had wire electrical discharge machining been used.

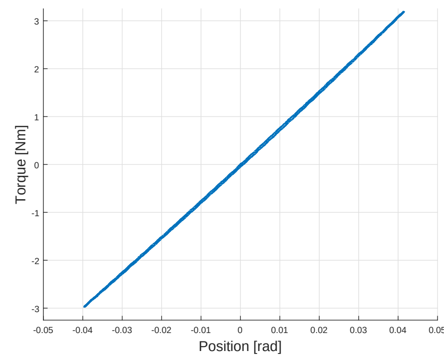


**FIGURE 5**. Determination of the spring rate (75.96 N·m/rad), which was estimated with a high coefficient of determination ($R^2$ = 0.9998).

## 3 Control

Control of the 1-DOF Bowden cable series elastic actuation module was performed through real-time software in a Matlab-Simulink Real-Time model communicating with Quanser's Q8 USB data acquisition board, which was run at a sampling rate of 1000 Hz. Velocity estimates of encoder positions were obtained through the Q8's built-in instantaneous velocity estimator, which runs at 100 MHz. Analog voltage commands from the Q8-USB were sent to two servo amplifiers (Advanced Motion Controls AMC 12A8) which converted the voltage commands to current control the brushed DC motors.

The control experiments presented demonstrate the performance necessary for the intended assessment of wrist passive stiffness and active range of motion. Based on previous passive wrist assessment [7], we determined that the device must be able to position control its joints to follow constant low-velocity trajectories (i.e., ramp position trajectories). For assessing active range of motion, the user backdrives the device. To achieve this, the device must be controlled through zero force control. In this assessment, the device should not adversely affect measured active range of motion due to excessive interaction torque between the device and user. Since no active wrist device has been used to measure active wrist range of motion, no benchmark for this interaction torque exists, but in this work we compare our results to the torque required to backdrive previous wrist devices.

### 3.1 Position Control

Position control of the module is achieved through PD control with feed-forward torque compensation of static friction. This feed-forward torque was estimated as the torque required to pull the cable at the output pulley through the Bowden cable transmission. Feed-forward compensation of friction was found to significantly improve the initial portion of the position control trajectory, as oscillations introduced from backlash and friction were reduced.

Due to the use of two motors for a single-DOF, the module is over-actuated; however, since the cables only produce rotational motion of the output pulley when under tension, only one motor can move the output joint in a given direction. As such, for the constant velocity needed in the stiffness assessment experiments, each joint consisted of a leader and follower motor. The lead motor was commanded to follow the desired position control trajectory through PD control and feed-forward friction compensation. On the other hand, the follower motor was sent a constant negative torque command, as found from preliminary experiments, which provided enough current to keep sufficient slack in the cable. This resulted in the lead motor not having to overcome friction present in both Bowden cable transmissions, and to have to backdrive the other motor.

To demonstrate that the device can realize the position control required for the intended application of measuring passive wrist stiffness [7, 8], an experiment was performed with the device unloaded and commanded to follow a ramp trajectory with a rate of 0.2 rad/s over a large range of motion. For the experiment, gains of $k_p = 20$ N·m/rad and $k_d = 0.1$ N·ms/rad, were selected as in [7, 8] to limit oscillations while achieving sufficient accuracy. The resulting average position error over the experiment was $e_{avg} = 0.014$ rad with a maximum error of $e_{max} = 0.029$ rad, indicating that the device was able to track the desired trajectory closely (see Fig. 6). Additionally, the joint velocity was an average of 0.181 rad/s, which although is 10% different than desired, is acceptable for the proposed use of the module [7, 8].

### 3.2 Zero Force Control

Due to the high static friction as a result of the Bowden cable transmission, to achieve zero force control, a controller which leverages the capabilities of the device to perform actuator position control was chosen [22]. In the force control approach presented in [22], to regulate torque, the motor attempts to control deflection of the spring through position control of the spring's

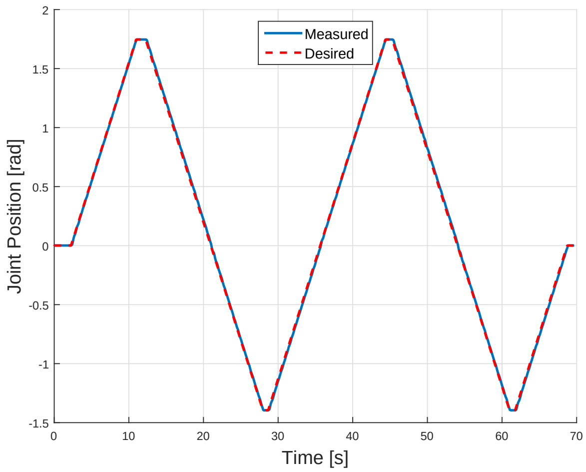


**FIGURE 6**. Position control performance of the 1-DOF module. The device is able to closely follow the desired trajectory, with sufficient accuracy for the intended application. For a right-handed user, positive values are in the direction of wrist flexion, while negative values are in the direction of wrist extension.

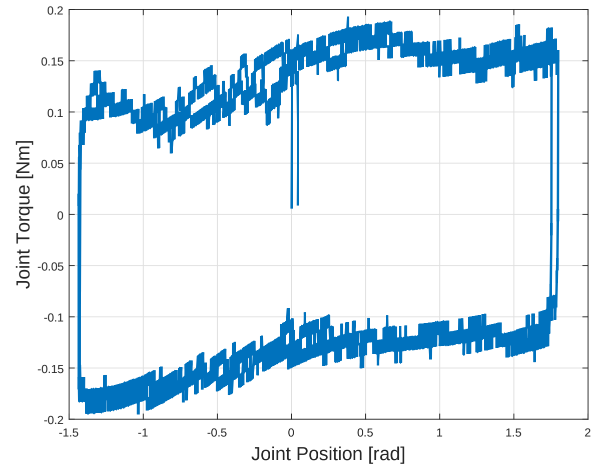


**FIGURE 7**. Zero force control experiment with the 1-DOF module. The plot illustrates that, despite geared motors and a Bowden cable transmission, the user is able to backdrive the device with perceived friction levels comparable to friction in other wrist exoskeletons [11, 16]. Note the torque signal's quantization of 12 N·mm as a result of the spring rate and encoder resolution.

input position. As in all series elastic devices, the module cannot regulate arbitrarily low torque since it has a practical lower bound based on the torque resolution of the spring. Additionally, to overcome backlash, the device's default state in this control mode is to provide tension on both sides of the spring such that the user can create a torque to inform the controller to perform active zero force control. Once a deadzone limit is exceeded, the zero force controller is used.

To illustrate the effectiveness of this zero force control approach for the module, an experimenter moved the device at a pace similar to that expected during the range of motion portion of the case study while moving the device through a large range of motion. The average velocity during the experiment was 0.313 rad/s with a maximum velocity of 0.729 rad/s. The zero force controller used PD gains of $k_p = 175$ N·m/rad and $k_d = 0.1$ N·ms/rad, as well as a deadzone of $\tau = 0.15$ N·m. The proportional gain was chosen for accurate tracking while maintaining stable interactions for a comfortable user bandwidth. The results of this experiment are shown in Fig. 7. Due to the zero force control, the spring torque during the experiment was low with $\tau_{avg}$ = 0.128 N·m and a maximum absolute torque of $\tau_{max}$ = 0.195 N·m. Considering this torque is similar to the interaction torque found in backdrivable wrist exoskeletons [11, 16], it is acceptable for enabling assessment of wrist range of motion.

## 4 Case Study Using 1-DOF Module

In this section a case study of an experimenter using the device in the intended wrist assessment for 1-DOF wrist flexion/extension is presented. The study demonstrates the feasibility of using the module for wrist passive stiffness and active range of motion assessment. Safety of the experimenter was ensured through first determining active range of motion and then operating the device based upon the determined range of motion through position control with software limits.

### 4.1 Methods

To estimate passive wrist stiffness, the user must attempt to relax their muscles while being moved by the module. To measure passivity, two bipolar surface electromyography (sEMG) electrodes were used. Each sEMG electrode was located on the user's forearm to measure muscle activity related to wrist flexion and extension, using electrode placements similar to [23] (see Fig. 8). As in [8], after donning the sEMG electrodes the experimenter performed three maximum voluntary contractions to serve as a reference for resting-state muscle activity.

The next portion of the experiment was to determine the experimenter's active range of motion. In this portion of the experiment, the user backdrove the robot through the zero force controller presented in Section 3.2. The experiment went to the flexion limit, and then the extension limit, repeating this process for three measurements of range of motion in each direction. The maximum flexion and extension values were collected and stored, since they were then used to control the robot for the passive wrist stiffness measurement.

To determine passive wrist stiffness, the robot was position controlled (see Section 3.1). The position limits set for the con-

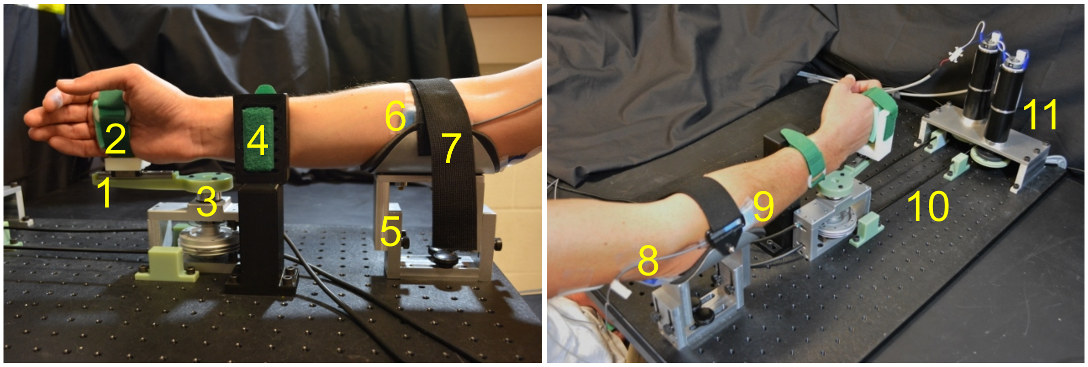


**FIGURE 8**. Experimental setup for the case study. 1) Passive linear bearing for wrist alignment, 2) open hand attachment, 3) 1-DOF module, 4) distal wrist cuff, 5) forearm support, 6) flexion electrode, 7) forearm cuff, 8) ground electrode, 9) extension electrode, 10) Bowden cables, and 11) motors.

troller were 90% of the user's maximum range of motion, providing a thorough characterization of wrist stiffness. During the experiment, sEMG activity was recorded to provide a measure of wrist passivity. The signals from the sEMG electrodes were processed digitally through a first order high-pass Butterworth filter with a 20 Hz cutoff frequency, a rectifier, and a a first-order low-pass Butterworth filter with a 2 Hz cutoff frequency, as in [24, 25]. The processed sEMG recordings were displayed to the user during the experiment to help maintain muscle passivity. After the experiment, the processed signals were normalized to the maximum voluntary contraction of each muscle.

### 4.2 Results

The experimenter's range of motion was 1.38 rad in flexion and 1.15 rad in extension. These values were used to provide the position limits, 90% of maximum range of motion, for the passive wrist stiffness experiment. The user position, torque, velocity, and muscle activity from this experiment are plotted in Fig. 9. As can be seen, the device was able to accurately track the ramp position trajectories. This lead to providing relatively constant velocity as necessary for accurately evaluating passive wrist stiffness to negate any potential affects of unmeasured wrist damping. Additionally, the processed muscle activity, normalized to maximum voluntary contraction, was relatively low ($<$5% of maximum voluntary contraction) throughout the experiment,

The passive wrist stiffness of the experimenter is shown in Fig. 10 through a torque vs. displacement plot. The wrist stiffness is relatively linear at first, but as the wrist is brought closer to the extremes of its range of motion, the stiffness increases. Additionally, we observed resistance at the onset of movement, and stretch relaxation in between outbound and inbound movements [8, 26]. As in previous studies [8], to identify passive wrist stiffness the linear portion of the stiffness profiles, as can be observed within approximately -0.5 to 1 rad in Fig. 10, were extracted for analysis. In this case, the data were segmented with respect to wrist flexion and extension, as well as for outbound and inbound movements. The first 0.1 rad of data were removed to eliminate short range stiffness effects, and the ends were segmented to 1.035 rad for flexion and -0.5 rad for extension.

The resulting mean stiffness values for the three trials for wrist flexion were found to be 0.44 N·m/rad ($R^2$ = 0.9892) for outbound movements and 0.25 N·m/rad ($R^2$ = 0.9607) for inbound movements. For wrist extension, the mean stiffness values were 0.27 N·m/rad ($R^2$ = 0.8573) for outbound movements and 0.2 N·m/rad ($R^2$ = 0.9246) for inbound movements. The $R^2$ values were obtained through a multiple-linear regression of torque and displacement using a linear model.

## 5 Discussion and Conclusions

This work presents a demonstration of a Bowden cable-based series elastic actuated 1-DOF wrist flexion/extension module. The module used in this work is the same module which will be used in a 2-DOF device to assess wrist passive stiffness and active range of motion, providing an important first step towards the control, evaluation, and application of the 2-DOF device, which has already been built and assembled. To facilitate these assessments, the module uses a Bowden cable transmission for increased range of motion, as well as series elastic actuation for direct torque measurement and transparent zero force control.

In this paper, details of the spring design and characterization were presented. The spring was found to be highly linear, providing an accurate estimate of user torque. Experimental validation of the 1-DOF module's position and zero force control capabilities were presented. The device was able to accurately track ramp position profiles with sufficient accuracy for evaluating passive wrist stiffness. The zero force control experiment demonstrated that minimal backdrive torque was required from the user, enabling the assessment of active range of motion.

A case study demonstrated the intended use of the 1-DOF

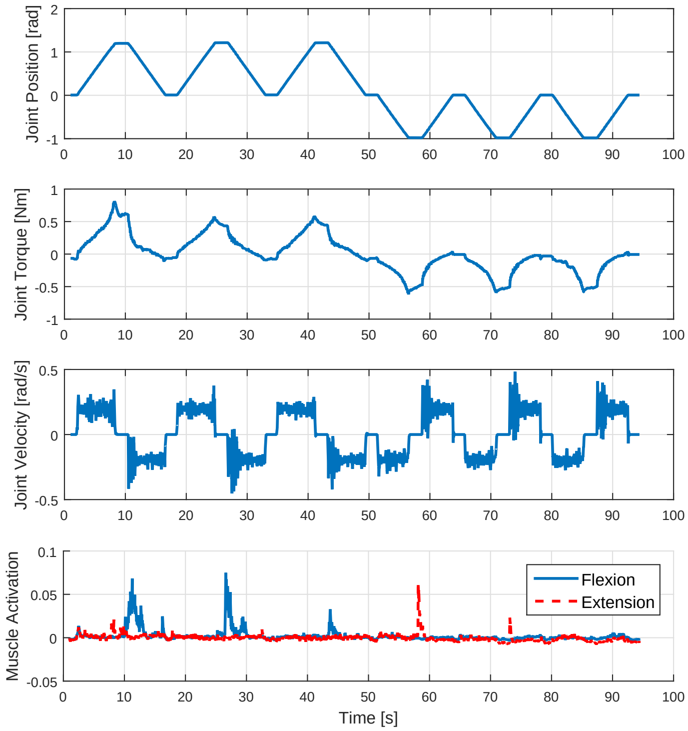


**FIGURE 9**. Relevant data collected during the stiffness portion of the case study. The plots (read from top to bottom) include user: joint position, joint torque, joint velocity, and muscle activity (normalized to maximum voluntary contraction for each corresponding muscle). The device was able to regulate the desired 0.2 rad/s velocity well, and the experimenter was able to regulate sEMG activity to in general be less than 5% of maximum voluntary contraction.

wrist flexion/extension module, finding the user's active range of motion and passive stiffness. Future work could analyze the nonlinear portions of the wrist stiffness profiles, which could be useful for wrist biomechancs modeling as well as bioinspired designs. Extension of the actuation module to 2-DOF wrist movements could deliver an important tool for clinicians, neuroscientists, and physical therapists. By incorporating quantitative assessments of human joint properties into the rehabilitation protocol, we can further our understanding of recovery after neurological injury in pursuit of optimal-patient-specific rehabilitation.

While the 1-DOF module was presented for robot-aided assessment, other wrist applications could leverage the actuation, transmission, and structural architecture due to its ease of scalability. The design can be readily scaled since the motors are located off-board and the spring is readily customizable. As a sample application, the module might be re-designed with softer springs and lower torque motors for haptic applications requiring lower intertia than wrist robots which locate the motors on board.

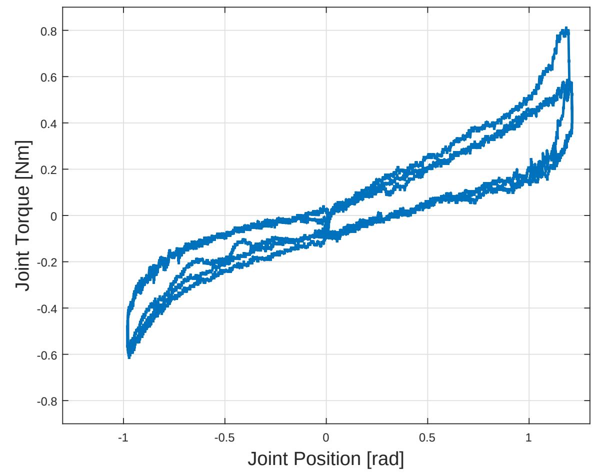


**FIGURE 10**. Wrist stiffness represented through a torque vs. displacement trajectory. The wrist's stiffness can be characterized as locally linear, while exhibiting a nonlinear transition region towards the range of motion limits, after which stiffness can possibly again be characterized through a linear relationship of torque and displacement.

## ACKNOWLEDGMENT


The authors thank Evan Pezent and Logan Farrell for their feedback on the design of the actuation module. The authors also thank Mikaela Juzswik, Tiffani Tjandra, and Saad Yousaf for their assistance in rapid prototyping parts for the module. Finally, the authors thank our machine-shop technician Mr. Joseph Gesenhues for his support in manufacturing the module.

This work was supported in part by the NSF GRFP No. 1450681, the NSF Integrative Graduate Education and Research Traineeship No. 1250104, the Dr. Eugene Alford Robotics Grant No. 017-102, and the Rice University IBB Hamill Innovation Award Grant.


## REFERENCES


[1] Babaiasl, M., Mahdioun, S. H., Jaryani, P., and Yazdani, M., 2015. "A review of technological and clinical aspects of robot-aided rehabilitation of upper-extremity after stroke". *Disability and Rehabilitation: Assistive Technology,* ***11***(4), pp. 263–280.

[2] Volpe, B., Krebs, H., Hogan, N., Edelstein, L., Diels, C., and Aisen, M., 2000. "A novel approach to stroke rehabilitation robot-aided sensorimotor stimulation". *Neurology,* ***54***(10), pp. 1938–1944.

[3] Loureiro, R. C., Harwin, W. S., Nagai, K., and Johnson, M., 2011. "Advances in upper limb stroke rehabilitation: a technology push". *Medical & Biological Engineering & Computing,* ***49***(10), p. 1103.

[4] Maggioni, S., Melendez-Calderon, A., van Asseldonk, E.,

Klamroth-Marganska, V., Lünenburger, L., Riener, R., and van der Kooij, H., 2016. “Robot-aided assessment of lower extremity functions: A review”. *Journal of Neuroengineering and Rehabilitation,* ***13***(1), p. 72.
[5] Fugl-Meyer, A. R., Jääskö, L., Leyman, I., Olsson, S., and Steglind, S., 1975. “The post-stroke hemiplegic patient: A method for evaluation of physical performance”. *Scandinavian Journal of Rehabilitation Medicine,* ***7***, pp. 13–31.
[6] Celik, O., O’Malley, M. K., Boake, C., Levin, H. S., Yozbatiran, N., and Reistetter, T. A., 2010. “Normalized movement quality measures for therapeutic robots strongly correlate with clinical motor impairment measures”. *IEEE Transactions on Neural Systems and Rehabilitation Engineering,* ***18***(4), pp. 433–444.
[7] Formica, D., Charles, S. K., Zollo, L., Guglielmelli, E., Hogan, N., and Krebs, H. I., 2012. “The passive stiffness of the wrist and forearm”. *Journal of Neurophysiology,* ***108***(4), pp. 1158–1166.
[8] Pando, A. L., Lee, H., Drake, W. B., Hogan, N., and Charles, S. K., 2014. “Position-dependent characterization of passive wrist stiffness”. *IEEE Transactions on Biomedical Engineering,* ***61***(8), pp. 2235–2244.
[9] Charles, S. K., and Hogan, N., 2011. “Dynamics of wrist rotations”. *Journal of Biomechanics,* ***44***(4), pp. 614–621.
[10] Squeri, V., Masia, L., Giannoni, P., Sandini, G., and Morasso, P., 2014. “Wrist rehabilitation in chronic stroke patients by means of adaptive, progressive robot-aided therapy”. *IEEE Transactions on Neural Systems and Rehabilitation Engineering,* ***22***(2), pp. 312–325.
[11] Krebs, H. I., Volpe, B. T., Williams, D., Celestino, J., Charles, S. K., Lynch, D., and Hogan, N., 2007. “Robot-aided neurorehabilitation: A robot for wrist rehabilitation”. *IEEE Transactions on Neural Systems and Rehabilitation Engineering,* ***15***(3), pp. 327–335.
[12] Crisco, J. J., Heard, W. M., Rich, R. R., Paller, D. J., and Wolfe, S. W., 2011. “The mechanical axes of the wrist are oriented obliquely to the anatomical axes”. *Journal of Bone & Joint Surgery,* ***93***(2), pp. 169–177.
[13] Perry, J. C., Rosen, J., and Burns, S., 2007. “Upper-limb powered exoskeleton design”. *IEEE/ASME Transactions on Mechatronics,* ***12***(4), pp. 408–417.
[14] Snoek, G. J., IJzerman, M. J., Hermens, H. J., Maxwell, D., and Biering-Sorensen, F., 2004. “Survey of the needs of patients with spinal cord injury: Impact and priority for improvement in hand function in tetraplegics”. *Spinal Cord,* ***42***(9), pp. 526–532.
[15] Gupta, A., O’Malley, M. K., Patoglu, V., and Burgar, C., 2008. “Design, control and performance of RiceWrist: A force feedback wrist exoskeleton for rehabilitation and training”. *The International Journal of Robotics Research,* ***27***(2), pp. 233–251.
[16] Pehlivan, A. U., Sergi, F., Erwin, A., Yozbatiran, N., Francisco, G. E., and O’Malley, M. K., 2014. “Design and validation of the RiceWrist-S exoskeleton for robotic rehabilitation after incomplete spinal cord injury”. *Robotica,* ***32***(8), pp. 1415–1431.
[17] Veneman, J. F., Kruidhof, R., Hekman, E. E., Ekkelenkamp, R., Van Asseldonk, E. H., and Van Der Kooij, H., 2007. “Design and evaluation of the LOPES exoskeleton robot for interactive gait rehabilitation”. *IEEE Transactions on Neural Systems and Rehabilitation Engineering,* ***15***(3), pp. 379–386.
[18] Blumenschein, L. H., McDonald, C. G., and O’Malley, M. K., 2017. “A cable-based series elastic actuator with conduit sensor for wearable exoskeletons”. In IEEE International Conference on Robotics and Automation (ICRA), pp. 6687–6693.
[19] Pratt, G. A., and Williamson, M. M., 1995. “Series elastic actuators”. In IEEE/RSJ International Conference on Intelligent Robots and Systems (IROS), pp. 399–406.
[20] Stienen, A. H., Hekman, E. E., Prange, G. B., Jannink, M. J., Aalsma, A. M., van der Helm, F. C., and van der Kooij, H., 2009. “Dampace: Design of an exoskeleton for force-coordination training in upper-extremity rehabilitation”. *ASME Journal of Medical Devices,* ***3***(3), pp. 1–10.
[21] Wang, S., Wang, L., Meijneke, C., Van Asseldonk, E., Hoellinger, T., Cheron, G., Ivanenko, Y., La Scaleia, V., Sylos-Labini, F., Molinari, M., et al., 2015. “Design and control of the MINDWALKER exoskeleton”. *IEEE Transactions on Neural Systems and Rehabilitation Engineering,* ***23***(2), pp. 277–286.
[22] Mosadeghzad, M., Medrano-Cerda, G. A., Saglia, J. A., Tsagarakis, N. G., and Caldwell, D. G., 2012. “Comparison of various active impedance control approaches, modeling, implementation, passivity, stability and trade-offs”. In IEEE/ASME International Conference on Advanced Intelligent Mechatronics (AIM), pp. 342–348.
[23] McDonald, C. G., Dennis, T. A., and O’Malley, M. K., 2017. “Characterization of surface electromyography patterns of healthy and incomplete spinal cord injury subjects interacting with an upper-extremity exoskeleton”. In IEEE International Conference on Rehabilitation Robotics (ICORR), pp. 164–169.
[24] Ha, K. H., Varol, H. A., and Goldfarb, M., 2011. “Volitional control of a prosthetic knee using surface electromyography”. *IEEE Transactions on Biomedical Engineering,* ***58***(1), pp. 144–151.
[25] Erwin, A., and Sup IV, F. C., 2015. “A haptic feedback scheme to accurately position a virtual wrist prosthesis using a three-node tactor array”. *PloS one,* ***10***(8), pp. 1–17.
[26] Given, J., Dewald, J., and Rymer, W., 1995. “Joint dependent passive stiffness in paretic and contralateral limbs of spastic patients with hemiparetic stroke”. *Journal of Neurology, Neurosurgery & Psychiatry,* ***59***(3), pp. 271–279.